Region-Based Segmentation of Capillary Density in Optical Coherence Tomography Angiography

Wenxiang Deng[1,2], Michelle R. Tamplin[2,3], Isabella M. Grumbach[2,3], Randy H. Kardon[2,4], and Mona K. Garvin[1,2(✉)]

[1] Department of Electrical and Computer Engineering, The University of Iowa, Iowa City, IA, USA
mona-garvin@uiowa.edu
[2] Iowa City VA Health Care System, Iowa City, IA, USA
[3] Department of Internal Medicine, The University of Iowa, Iowa City, IA, USA
[4] Department of Ophthalmology and Visual Sciences, The University of Iowa, Iowa City, IA, USA

Abstract. Microvascular changes are one of the early symptoms of retinal diseases. Recently developed optical coherence tomography angiography (OCTA) technology allows visualization and analysis of the retinal microvascular network in a non-invasive way. However, automated analysis of microvascular changes in OCTA is not a trivial task. Current approaches often attempt to directly segment the microvasculature. These approaches generally have problems in cases of poor image quality and limited visibility of the vasculature. Evaluating the quality of the results is also challenging because of the difficulty of manually tracing the microvasculature, especially in cases of low image quality or with images with a larger field of view. In this work, we develop an automated deep-learning approach to assign each pixel within human OCTA *en-face* images the probability of belonging to a microvascular density region of each of the following categories: avascular, hypovascular, and capillary-dense. The AUCs (area under the receiver operating characteristic curves) were 0.99 (avascular), 0.93 (hypovascular), and 0.97 (capillary-dense) for segmenting each of the categories. The results show very good performance and enables global and region-based quantitative estimates of microvascular density even in relatively low-quality *en-face* images.

Keywords: OCT-Angiography · Capillary density · Deep learning

1 Introduction

The retinal microvascular network supplies the retina with oxygen and nutrition. Ocular diseases including diabetic retinopathy [1], glaucoma [2], age-related

H. Fu et al. (Eds.): OMIA 2019, LNCS 11855, pp. 18–25, 2019.
https://doi.org/10.1007/978-3-030-32956-3_3

macular degeneration [3], and radiation retinopathy [4,5] often show changes in the microvasculature. Traditionally, fluorescein angiography (FA) is widely used for assessing retinal micro-circulation. However, this technique is invasive and doesn't distinguish microvasculature in superficial retinal layers from the deeper plexus. OCT angiography (OCTA) is a modality increasingly used for assessing retinal vasculature pathologies in retinal studies [6–8].

Many existing approach for measuring capillary density from *en-face* OCTA images – including the use of fractal analysis [9,10], vessel enhancement filters [11], and a convolutional-neural-network approach [12] – attempt to first directly segment the microvasculature. However, because the quality of OCTA images varies and is susceptible to noise or artifacts, a direct measurement of vessels in OCTA *en-face* images is often not feasible. Figure 1 shows an example comparison of good quality *en-face* images (Fig. 1(a), (b)) and an image with a poorly visible microvascular network (Fig. 1(c)). These differences can be common in the analysis of patients with diseases such as radiation retinopathy [4].

Other strategies for providing an overall sense of vessel density from an OCTA *en-face* image include directly detecting the fovea avascular zone (FAZ) or non-FAZ avascular regions using filters and/or fractal analysis [13–15] and a recent deep-learning approach to detect avascular areas [16]. However, these approaches do not take into consideration of the possibility of reduced (but not completely avascular) capillary density in regions. Also, location-dependent artifacts are often not addressed.

(a) (b) (c)

Fig. 1. Example variability of OCTA *en-face* image quality. (a) An example image from a healthy subject showing vessels clearly. (b) and (c) are *en-face* images from the unaffected and affected eye of a patient with radiation retinopathy. (c) shows an image with a lower signal-to-noise ratio (SNR) and less visible capillaries.

In this work, to address the frequent limited visibility of individual capillaries in OCTA images but to also allow for characterization of differing density levels at each pixel, we train and evaluate a deep-learning-based approach (using a modified U-net architecture) to segment avascular, hypovascular, and capillary-dense areas from OCTA *en-face* images. We train and evaluate our approach (using 10-fold cross-validation) on a challenging dataset of uveal melanoma

patients (including those with radiation retinopathy) and controls whereby, as shown in Fig. 1, the visibility of the capillaries can vary substantially.

2 Methods

2.1 Preprocessing

In each OCTA scan we use in this work, there is a volumetric structural OCT scan showing the macular tissue and a corresponding split spectrum amplitude-decorrelation angiography (SSADA) scan showing the vesselness. We use the raw OCT and SSADA data to segment and form the *en-face* projection angiogram of superficial layers. More specifically, to obtain the layer information, a graph-based layer segmentation algorithm [17] is used to segment the superficial layers in the corresponding OCT volumes. In this approach, we follow the definition from Camino et al. [18] and use the superficial layers as the combination of retinal nerve fiber layer (RNFL) to inner plexiform layer (IPL). Figure 2(a) shows the SSADA information overlaid on a b-scan in the segmented layers. To generate the projection images, we use the maximum intensity in each column in these layers. An example result can be seen in Fig. 2(b).

Because the deep learning approach we use prefers pixel dimensions divisible by 32, the generated *en-face* images are also unified to dimensions of 480×480 by upsampling with cubic spline interpolation to preserve more details.

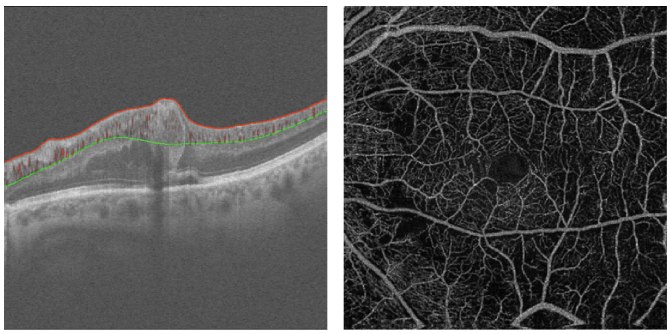

(a) (b)

Fig. 2. An example OCTA image. (a) OCT b-scan showing the superficial layers used in this study. The superficial layers are shown between the red and green boundaries, and only the SSADA information shown in red scatters between the boundaries are used. (b) The *en-face* projection angiogram of the superficial layers of the structural OCT volume indicated in (a). (Color figure online)

2.2 Input Data Generation

For the input of our deep network, in addition to the *en-face* images, to help the network deal with potential location-specific artifacts, such as signal dropout on the temporal side (Fig. 3(a)), we also provide a radial location map (providing the distance from the center), as shown in Fig. 3(c), and a temporal-to-nasal location map (providing the distance from the temporal side), as shown in (Fig. 3(d)). By providing such additional inputs, we can help to avoid results such as that in Fig. 3(b) whereby the regions with signal dropout would incorrectly be classified as avascular or hypovascular regions.

In the training stage, rotation, flipping, and cropping are applied to each input image before each training iteration. The original *en-face* image is first is augmented with random rotations in range $(-180°, 180°)$. A random horizontal flip is then applied. The training image is then randomly cropped to a fixed size of 256×256 pixels and, to further help address the possibility of regional signal dropout, a local contrast change is also applied.

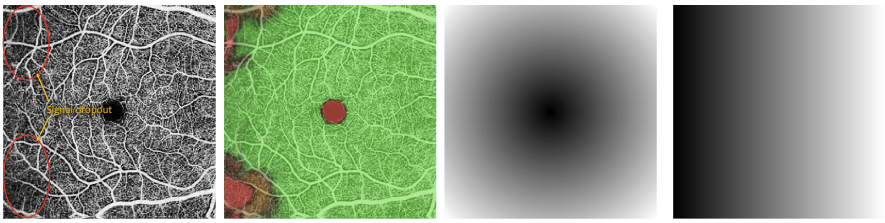

Fig. 3. Motivation for use of location maps as additional input. (a) OCTA *en-face* image from a healthy control subject with local signal dropout on temporal side. (b) Segmentation result without additional location-specific maps as input. (c) Radial location map. (d) Temporal-to-nasal location map.

2.3 Network Structure

Here, we develop a fully automated deep-learning based approach. A modified version of U-Net [19] is applied to do a pixel-based separation of avascular regions, hypovascular regions (i.e., regions with capillary dropout) and capillary-dense regions. The overall network structure of this work is shown in Fig. 4. The inputs are the *en-face* image and two location maps as discussed above and the outputs are three probability maps for the avascular region, hypovascular region, and capillary-dense region.

Our modifications to the original U-net are, in part, inspired by recent work by Iglovikov et al. [20] that showed that using a deeper VGG11 network as the encoder can increase the segmentation accuracy compared to the original U-Net. Here we use a similar network structure. We also add batch normalization (BN)

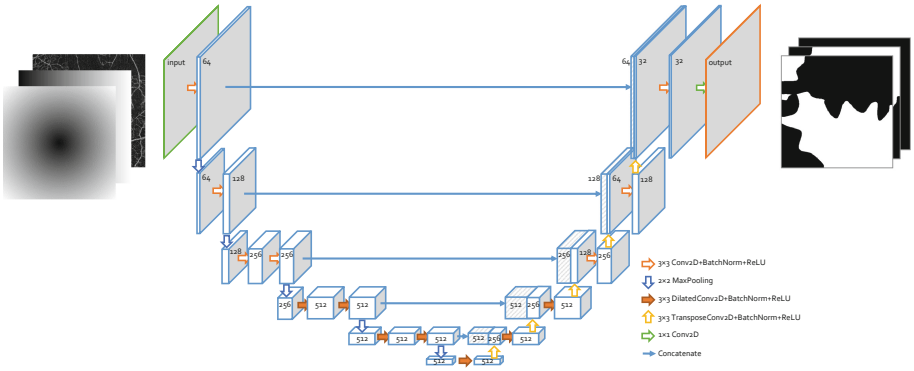

Fig. 4. The modified version of U-Net with dilated convolutions used in this work.

layers [21] to improve the numerical stability. Another modification is changing the convolutions in some of the layers to be dilated convolutions introduced by Yu et al. [22]. This convolution model enables a larger receptive field for the network without requiring additional parameters to be learned. Therefore, we change the conventional 3×3 convolutions in some layers of the U-Net to 3×3 with a dilation factor of 2.

For the loss function, a combination of binary cross-entropy (BCE) loss and Dice loss is used, thus we can simultaneously maximize the per-pixel prediction as well as the overall intersection between the predicted probability maps and the manual tracing.

3 Experiments and Results

A total of 166 macular OCTA scan sets (structural OCT volumes and corresponding SSADA data) acquired with AngioVue (Optovue, Inc., Fremont, CA) from 59 human subjects are used in the study. Within the subjects, 43 are uveal melanoma patients and 16 are control cases. All procedures involving human subjects in this study were approved by the Institutional Review Boards (IRB) and the Human Subjects Office at the University of Iowa.

The OCT volumes and SSADA scans from all control subjects and 37/43 uveal melanoma subjects have dimensions of $400 \times 400 \times 640$ and $400 \times 400 \times 160$, respectively, corresponding to physical dimensions of $6\,\text{mm} \times 6\,\text{mm} \times 2\,\text{mm}$. The OCT volumes and SSADA scans from the remaining six uveal melanoma subjects have dimensions of $304 \times 304 \times 640$ and $304 \times 304 \times 160$, respectively. As mentioned in Sect. 2.1, all the generated *en-face* images are rescaled to a unified size of 480×480 before further processing. For training and evaluation purposes, the capillary-dense regions, hypovascular (capillary dropout) and avascular regions are also manually identified in each *en-face* image.

To train the network, we use Adam optimizer to train the network from scratch, with an initial learning rate of 1e-4. The learning rate changed to 1e-5

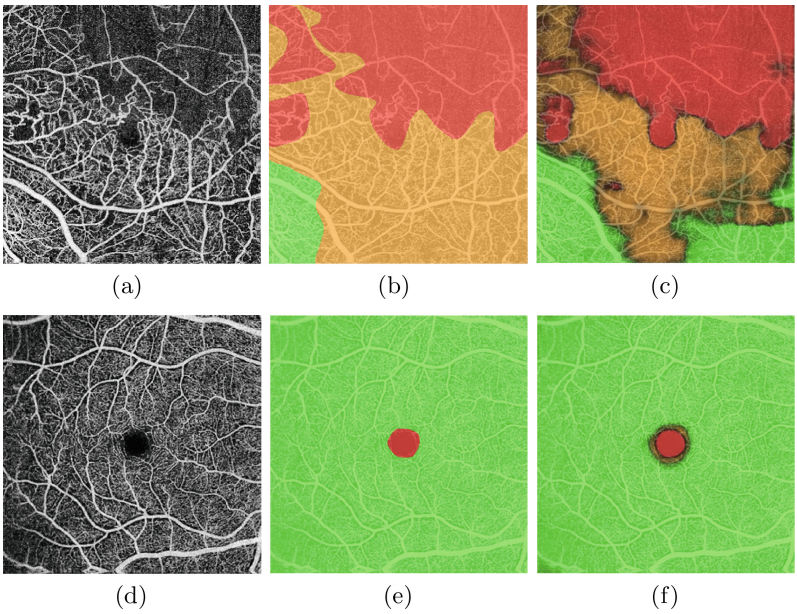

Fig. 5. Example results from the proposed deep-learning approach. (a–c) show an example result from a radiation retinopathy patient, and (d–f) are for a control subject. (a), (d) The *en-face* OCTA image (enhanced for increased visibility). (b), (e) The manual tracing for the image. (c), (f) The segmentation result of the three classes. Red = avascular. Orange = hypovascular. Green = capillary-dense. (Color figure online)

after 500 epochs and 1e-6 at 700 epochs. A total of 1000 epochs are used for the total training on a single Nvidia GeForce 1080 Ti GPU. It takes around 3 hours to train one network, and approximately a day to train all the U-Nets for the cross-validation experiment. In the testing phase, for each 480×480 *en-face* image, it takes about 0.1s to run on GPU and 3 s to run on a CPU. Because the U-net structure is fully convolutional, while training is performed with 256×256 cropped images, testing can be directly performed with 480×480 images.

To evaluate the results, area under the pixel-based receiver operating characteristic (ROC) curves (AUC) are used in a 10-fold cross-validation approach. The first nine folds each have images from 53 randomly chosen subjects as the training set and images from 6 subjects as the test set. The remaining fold has 54 subjects for training and 5 for testing. Among the ROCs, the prediction of avascular regions has the best performance, with an AUC of 0.99 and the prediction of the capillary-dense regions has the second-best performance, with an AUC of 0.97. The hypovascular prediction generally gives a slightly lower AUC of 0.93. This is partially because the tracing is more subjective than the tracing of avascular areas as it is sometimes hard to distinguish hypovascular regions.

An example of the original image, the manual tracing, and the corresponding result can be seen in Fig. 5. Visually, this approach offers clean predictions for

avascular regions marked in red. In fact, the regions are slightly more consistent and detailed than manual tracings. On the other hand, the predicted hypovascular regions in orange are less confident and have some misclassified regions.

4 Discussion and Conclusions

In this work, we develop a region-based segmentation method to identify different microvascular densities within OCTA *en-face* projection images. A deep neural network is used to simultaneously find these categories. The first main contribution of this work is that by tracing and training on OCTA *en-face* images as different density regions, we can avoid the difficulty to distinguish individual capillaries giving us the ability to still obtain density estimates on lower-quality OCTA images where individual vessels are not visible. The second contribution is that by adding additional location maps to the inputs of the deep learning network, the segmentation network can successfully avoid some OCTA artifacts to generate better results. To the best of our knowledge, this trained deep-learning approach is the first fully automated approach to categorize multiple levels of vascular density in OCTA images. The results show very accurate predictions for the avascular and normal regions in uveal melanoma patients and a slightly lower accuracy in predicting hypovascular regions.

Acknowledgements. This work was supported, in part, by the VA Center for the Prevention and Treatment of Visual Loss, AHA 18IPA34170003, and NIH T32 CA078586.

References

1. Chen, Q., et al.: Macular vascular fractal dimension in the deep capillary layer as an early indicator of microvascular loss for retinopathy in type 2 diabetic patients. Invest. Ophthalmol. Vis. Sci. **58**(9), 3785–3794 (2017)
2. Flammer, J., et al.: The impact of ocular blood flow in glaucoma. Prog. Retinal Eye Res. **21**(4), 359–393 (2002)
3. Jia, Y., et al.: Quantitative optical coherence tomography angiography of choroidal neovascularization in age-related macular degeneration. Ophthalmology **121**(7), 1435–1444 (2014)
4. Veverka, K.K., AbouChehade, J.E., Iezzi Jr., R., Pulido, J.S.: Noninvasive grading of radiation retinopathy: the use of optical coherence tomography angiography. Retina **35**(11), 2400–2410 (2015)
5. Shields, C.L., Say, E.A.T., Samara, W.A., Khoo, C.T., Mashayekhi, A., Shields, J.A.: Optical coherence tomography angiography of the macula after plaque radiotherapy of choroidal melanoma: comparison of irradiated versus nonirradiated eyes in 65 patients. Retina **36**(8), 1493–1505 (2016)
6. Spaide, R.F., Klancnik, J.M., Cooney, M.J.: Retinal vascular layers imaged by fluorescein angiography and optical coherence tomography angiography. JAMA Ophthalmol. **133**(1), 45–50 (2015)
7. Giannakaki-Zimmermann, H., Kokona, D., Wolf, S., Ebneter, A., Zinkernagel, M.S.: Optical coherence tomography angiography in mice: comparison with confocal scanning laser microscopy and fluorescein angiography. Transl. Vis. Sci. Technol. **5**(4), 11–11 (2016)

8. Chen, J.J., AbouChehade, J.E., Iezzi Jr., R., Leavitt, J.A., Kardon, R.H.: Optical coherence angiographic demonstration of retinal changes from chronic optic neuropathies. Neuro-Ophthalmology **41**(2), 76–83 (2017). https://doi.org/10.1080/01658107.2016.1275703
9. Gadde, S.G., et al.: Quantification of vessel density in retinal optical coherence tomography angiography images using local fractal dimension. Invest. Ophthalmol. Vis. Sci. **57**(1), 246–252 (2016)
10. Zahid, S., et al.: Fractal dimensional analysis of optical coherence tomography angiography in eyes with diabetic retinopathy. Invest. Ophthalmol. Vis. Sci. **57**(11), 4940–4947 (2016)
11. Dongye, C., et al.: Automated detection of dilated capillaries on optical coherence tomography angiography. Biomed. Opt. Express **8**(2), 1101–1109 (2017)
12. Prentašić, P., et al.: Segmentation of the foveal microvasculature using deep learning networks. J. Biomed. Opt. **21**(7), 075008–075008 (2016)
13. Zhang, M., Hwang, T.S., Dongye, C., Wilson, D.J., Huang, D., Jia, Y.: Automated quantification of nonperfusion in three retinal plexuses using projection-resolved optical coherence tomography angiography in diabetic retinopathy. Invest. Ophthalmol. Vis. Sci. **57**(13), 5101–5106 (2016)
14. Sandhu, H.S., et al.: Automated diabetic retinopathy detection using optical coherence tomography angiography: a pilot study. Br. J. Ophthalmol. **102**(11), 1564–1569 (2018)
15. Anegondi, N., Chidambara, L., Bhanushali, D., Gadde, S.G., Yadav, N.K., Sinha Roy, A.: An automated framework to quantify areas of regional ischemia in retinal vascular diseases with OCT angiography. J. Biophotonics **11**(2), e201600312 (2018)
16. Guo, Y., Camino, A., Wang, J., Huang, D., Hwang, T.S., Jia, Y.: MEDnet, a neural network for automated detection of avascular area in OCT angiography. Biomed. Opt. Express **9**(11), 5147–5158 (2018)
17. Garvin, M.K., Abràmoff, M.D., Wu, X., Russell, S.R., Burns, T.L., Sonka, M.: Automated 3-D intraretinal layer segmentation of macular spectral-domain optical coherence tomography images. IEEE Trans. Med. Imaging **28**(9), 1436–1447 (2009)
18. Camino, A., et al.: Automated registration and enhanced processing of clinical optical coherence tomography angiography. Quant. Imaging Med. Surg. **6**(4), 391 (2016)
19. Ronneberger, O., Fischer, P., Brox, T.: U-Net: convolutional networks for biomedical image segmentation. In: Navab, N., Hornegger, J., Wells, W.M., Frangi, A.F. (eds.) MICCAI 2015. LNCS, vol. 9351, pp. 234–241. Springer, Cham (2015). https://doi.org/10.1007/978-3-319-24574-4_28
20. Iglovikov, V., Shvets, A.: TernausNet: U-Net with VGG11 encoder pre-trained on ImageNet for image segmentation. arXiv preprint arXiv:1801.05746 (2018)
21. Ioffe, S., Szegedy, C.: Batch normalization: accelerating deep network training by reducing internal covariate shift. In: International Conference on Machine Learning, pp. 448–456 (2015)
22. Yu, F., Koltun, V.: Multi-scale context aggregation by dilated convolutions. arXiv preprint arXiv:1511.07122 (2015)